

JAMSTEC *Chikyu* SCORE Expedition 912 Leg 2

Preliminary Cruise Report

Cycle of catastrophic caldera-forming eruption and spread out ignimbrite at Kikai submarine caldera

Yoshiyuki Tatsumi (Kobe Univ.), Katsuya Kaneko (Kobe Univ.),
Natsumi Okutsu (JAMSTEC), Kan Aoike (JAMSTEC) and the Exp.912-Leg.2 Shipboard Scientists



Acknowledgements

Expedition 912 shipboard scientists thank all the MQJ drilling staff and MWJ laboratory technical staff of the D/V *Chikyu* for the wonderful cruise and taking high-quality core samples. Special thanks MarE3 Operation Superintendent of the expedition, for successful sampling. The proponents would like to thank J-DESC and MarE3 for providing the opportunity of this short expedition.

Contents

1. Cruise Information	4
2. Expedition 912 Leg.2 Shipboard scientists	4
3. Introduction	6
4. Scientific objectives	6
5. Geological background	6
6. Shipboard core analysis flow.....	8
7. Operation	10
8. Cruise Log	12
9. Method and result of onboard research activities	16
9.1. X-ray computed tomography	16
9.2. Physical properties measurements of whole-round core with the Multi-Sensor-Core-Logger	18
9.3. Physical properties except for the MSCL-W measurement.....	20
9.4. Lithology	28
9.5. Paleomagnetism	30
10. Post-cruise study plan	30
11. References	31

1. Cruise Information

Cruise ID: CK20-S01, Exp. 912

Name of vessel: D/V Chikyu

Proposal representative: Yoshiyuki Tatsumi (Kobe Univ.)

Cruise period: Jan. 5th, 2020 - Jan. 15th, 2020

Leg period: Jan. 8th, 2020 – Jan. 15th, 2020

Ports of departure / arrival: Shimizu / Sasebo

2. Expedition 912 Leg.2 Shipboard scientists

Yoshiyuki Tatsumi (Chief scientist, Lead Proponent)

Kobe Ocean-bottom exploration center, Kobe University

1-1-5, Fukae-minami-cho, Higashi-nada-ku, Kobe 658-0022 Japan

Katsuya Kaneko (Physical Property Specialist, Sedimentologist)

Graduate school of Science, Kobe University

1-1, Rokkodai-cho, Nada-ku, Kobe 657-8501 Japan

Keiko Suzuki (Sedimentologist)

Kobe Ocean-bottom exploration center, Kobe University

1-1-5, Fukae-minami-cho, Higashi-nada-ku, Kobe 658-0022 Japan

Nobukazu Seama (Physical Property Specialist)

Graduate school of Science, Kobe University

1-1, Rokkodai-cho, Nada-ku, Kobe 657-8501 Japan

Yuzuru Yamamoto (Physical Property Specialist, Sedimentologist)

Graduate school of Science, Kobe University

1-1, Rokkodai-cho, Nada-ku, Kobe 657-8501 Japan

Koji Kiyosugi (Sedimentologist)

Kobe Ocean-bottom exploration center, Kobe University

1-1-5, Fukae-minami-cho, Higashi-nada-ku, Kobe 658-0022 Japan

Tetsuo Matsuno (Physical Property Specialist)

Kobe Ocean-bottom exploration center, Kobe University

1-1-5, Fukae-minami-cho, Higashi-nada-ku, Kobe 658-0022 Japan

Reina Nakaoka (Physical Property Specialist, Sedimentologist)

Kobe Ocean-bottom exploration center, Kobe University

1-1-5, Fukae-minami-cho, Higashi-nada-ku, Kobe 658-0022 Japan

Takeshi Hanyu (Physical Property Specialist, Sedimentologist)

Japan Agency for Marine-Earth Science and Technology

2-15, Natsushima-cho, Yokosuka 237-0061 Japan

Ryohei Kikuchi (Paleomagnetism)

Graduate school of Science, Kobe University

1-1, Rokkodai-cho, Nada-ku, Kobe 657-8501 Japan

Hiroto Yamaguchi (Paleomagnetism)

Graduate school of Science, Kobe University

1-1, Rokkodai-cho, Nada-ku, Kobe 657-8501 Japan

Natsumi Okutsu (Expedition Project Manager)

Japan Agency for Marine-Earth Science and Technology

2-15, Natsushima-cho, Yokosuka-city, Kanagawa, 237-0061, Japan

Kan Aoike (Sub Expedition Project Manager)

Japan Agency for Marine-Earth Science and Technology

2-15, Natsushima-cho, Yokosuka-city, Kanagawa, 237-0061, Japan

3. Introduction

Catastrophic caldera forming eruptions (CCFEs) that discharge more than 40 km^3 ($>M 7$; M , eruption magnitude) of Silica-rich magma as pyroclastics and lead to the huge caldera collapse are rare but extremely hazardous events; they also have severe global impacts such as ‘volcanic winter’ (Rampino et al., 1988). The Japanese Archipelago is one site of dense and frequent occurrence of CCFEs. A recent statistical approach (Tatsumi and Suzuki-Kamata, 2014) suggested a $\sim 1\%$ probability of a CCFE in the next 100 years in Japan based on the eruption records. Furthermore, more than 100 million people live in an area potentially covered by ignimbrite and 10 cm thick tephra, from a CCFE. Estimating the eruption volume of pyroclastics is thus essential in evaluating the risk and cause of CCFE. The IODP science plan for 2013-2023 clearly mentioned the importance of hazards on human time scales such as earthquake, tsunamis, and landslides. Although the science plan itself does not emphasize CCFE, the *Chikyu*+10 international workshop in 2013 included deep and shallow drilling at submarine caldera volcanoes as one important target by the *Chikyu*.

The ignimbrite, which is created by collapse of a huge eruption column being developed during a CCFE and spreads out widely in all directions from the supervolcano is the major ejecta of CCFEs.

4. Scientific objectives

A volume estimate of ignimbrite, especially non welded ash flow deposit, which is readily removed by post CCFE erosion, is difficult rather than that of co ignimbrite ash that tends to be well preserved in stratum. This expedition is aiming at precise volume estimation of an ignimbrite based on identification of the submarine deposit of the ignimbrite discharged from a submarine supervolcano by the *Chikyu* piston coring.

5. Geological background

The latest CCFE in the Japanese Archipelago occurred at 7.3 ka and created the Kikai submarine caldera of the south of Kyushu Island (Fig. 1). This Kikai Akahoya CCFE is one of the three largest eruptions in Japan for the last 120 ky. Kikai caldera with a size of $19 \times 22 \text{ km}$ is located in the East China Sea to the south of the Kyushu Island and lies astride the volcanic front of the SW Japan arc that is built by subduction of Philippine Sea plate at Nankai trough and Ryukyu trench (Fig. 1). This caldera is created in the southern extension of the Kagoshima graben across the southernmost part of Kyushu Island and exhibits a double caldera structure (Fig. 1). Two islands, Take shima and Satsuma Iwo jima, represent subaerial parts of the northern rim of this submarine caldera (Fig. 1). Two post caldera stratovolcanoes, Iwo dake and Inamura dake with a volume of 1.1 and 0.1 km^3 , respectively, are developed on Satsuma Iwo jima Island (Ono et al., 1982). At least three supereruptions, Koabi, Kikai Tozurahara, and Akahoya eruptions occurred at 140, 95 and 7.3 ka, respectively, in this caldera

(Ono et al., 1982; Machida et al., 2001; Maeno and Taniguchi, 2007). Significant cooling event due to Kikai Akahoya eruption was not clearly caught by high resolution paleoclimate archives. However, it is reported that Koya ignimbrite caused damage to vegetation in southern Kyusyu for about two hundred years (Matsushita, 2002). Recent surveys by Kobe University R/V Fukae-Marui, including multi-beam mapping of the volcano morphology, side-scan sonar acoustic and ROV imaging, multiscan sonar acoustic and ROV imaging, multi-channel seismic reflection survey, and rock sampling by dredging and diving,

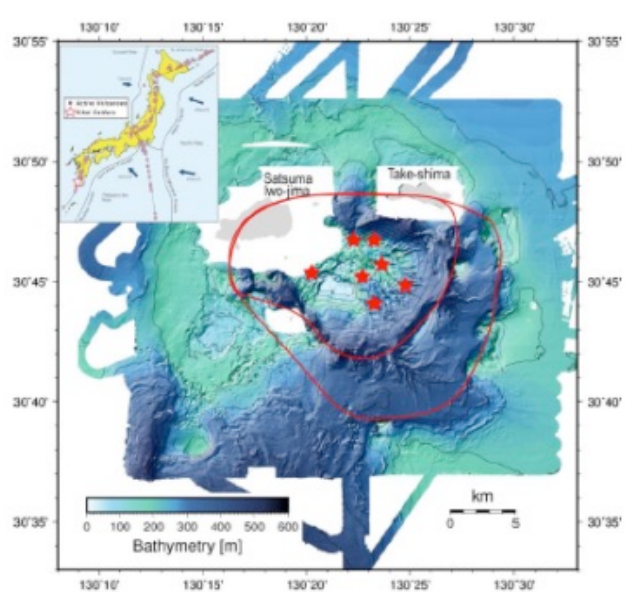


Fig. 1 Location and bathymetry of Kikai caldera, which exhibits a double caldera structure (red lines). Within the inner caldera, a giant rhyolitic lava dome is situated on the caldera floor. This dome is active as several water column anomalies (red stars) are found. Koya ignimbrite produced by the 7.3-ka CCFE may form the smooth and gentle slope outside the outer caldera.

confirmed that a giant rhyolitic lava dome is situated on the inner caldera floor, i.e., by a post-CCFE magmatic activity and it exhibits several water column anomalies (Tatsumi et al., 2018). This suggests that an active large magma plumbing system is lurking beneath this volcano even at this post caldera stage. In order to understand the caldera cycle evolution and further to predict a future CCFE in this supervolcano, therefore, the volume of ignimbrite discharged at 7.3 ka CCFE, Koya ignimbrite, is needed.

The 7.3 ka Koya ignimbrite, is widely distributed over the proximal/adjacent islands and the mainland of southern Kyushu. It has been suggested that this ignimbrite shows a rather low aspect ratio with rather thin (< 2 m) and wide (~100 km) deposition (Ui, 1973), which provided a volume estimate for this ignimbrite (50 km³). However, our recent on land survey revealed that both the ignimbrite thickness and the maximum pumice size tend to decrease with increasing the distance across the sea (Fig. 2). This may lead to a hypothesis that a significant amount of pyroclastics including large pumices and ashes was lost during traveling over the sea and deposited on the sea floor. Revealing the mass of Koya ignimbrite derived pyroclastics on the sea floor should be thus a key to estimating the total volume of this ignimbrite.

Syn-caldera volcanics show different chemical trend from pre and post caldera volcanics such as stratovolcanoes and lava domes of Kikai supervolcano (Fig. 3). These chemical characteristics of Koya ignimbrite should provide a better chance for discrimination of this ignimbrite from other ejecta.

The geochemical characteristics may suggest that felsic magma of both pre and post caldera stages were produced by partial melting of the lower crust and rose and accumulated in upper crust to form

a large magma reservoir with crystal mush. Voluminous felsic magma generation in Kikai Akahoya eruption can be explained by rejuvenation of crystal mush when a mantle derived mafic magma penetrated crystal mush. The systematic difference in chemical trends for Koya syn-caldera stage and other post caldera stage magma could be understood by depletion of incompatible elements in the lower crustal source via. Extraction of Koya felsic melts.

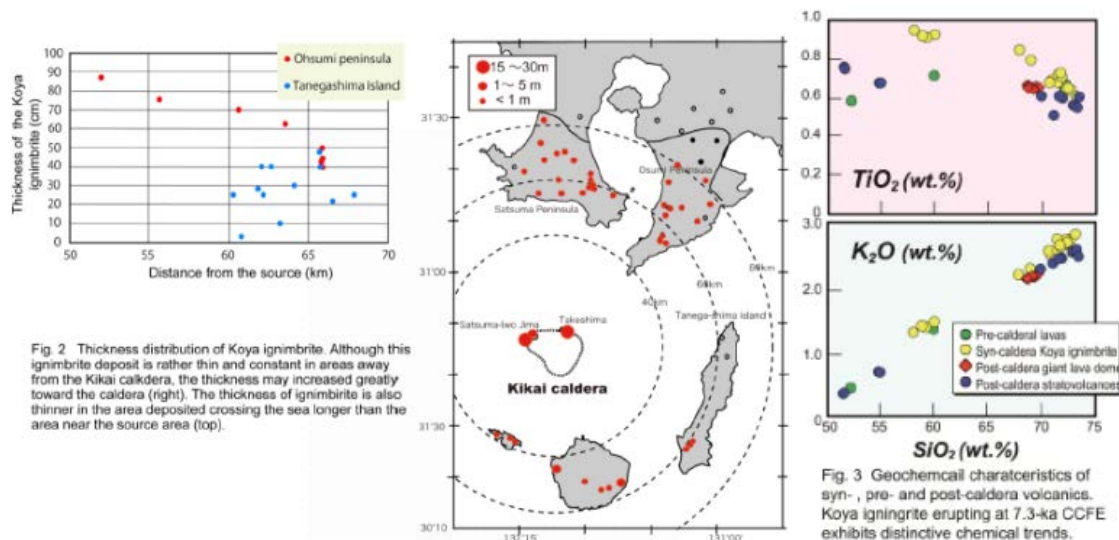


Fig. 2 Thickness distribution of Koya ignimbrite. Although this ignimbrite deposit is rather thin and constant in areas away from the Kikai caldera, the thickness may increase greatly toward the caldera (right). The thickness of ignimbrite is also thinner in the area deposited crossing the sea longer than the area near the source area (top).

Fig. 3 Geochemical characteristics of syn-, pre- and post-caldera volcanics. Koya ignimbrite erupting at 7.3-ka CCFE exhibits distinctive chemical trends.

6. Shipboard core analysis flow

Six holes were drilled for coring at Site C9036 (Table 1). All cores were taken by Hydraulic Piston Coring System (HPCS) and Short HPCS (S-HPCS) of the *Chikyu*. The HPCS is designed to take a 9.5 m-long core while the S-HPCS is a tool modified from the HPCS to take a shorter core of 4.5 m, 3 m or 1.5 m long. In this expedition, the 4.5 m-type S-HPCS was used.

Cores were then used for shipboard sampling and analysis. General core analysis flow is shown in Fig 4, and detailed protocol is described in 9. **Methods and results of onboard research activities.**

Cores retrieved on the deck were delivered to the Core Cutting Area generally about 30 minutes later after the retrieval. The recovered core length excluding lengths of obvious void spaces were then measured and the Drilling Operations team determined the penetration length (= advance) based on the drilling parameters, the recovered core length and the core condition. A core was cut into 1.4 m-long sections and each section length was entered into the J-CORES database, along with core identification information, drilling advance and depth information. Then each core sections were examined with the X-ray Computed Tomography (X-CT) scanner. After X-CT scanning, core sections were examined by the whole-round multisensory core logger (MSCL-W) for gamma ray attenuation (GRA) density, magnetic susceptibility (MS), and natural gamma radiation (NGR). Measurement intervals are described in 9.1. **Physical properties measurements of whole-round core with the Multi-Sensor-Core-Logger.** Subsequently, thermal conductivity was determined if the consolidation

state of the sediment allowed for the measurement.

After the MSCL-W scanning and thermal conductivity measurement, the core section was split lengthwise along the lines delimiting the archive and working halves. Archive-half sections were processed in the following way: digital images were taken with the photo image logger (MSCL-I) prior to visual core description (VCD) by shipboard scientists. Small amount of sample was taken from the archive half in areas of lithologic interest for smear slide analysis. After the VCD was completed, paleomagnetic measurements was conducted using the superconducting rock magnetometer (SRM) before the archive halves were prepared for storage.

For working-half sections, shipboard analysis of physical properties was conducted; vane shear test for half-round core, and discrete samples were taken for moisture and density measurements (MAD), P-wave velocity, and Impedance.

All half-round core sections were vacuum sealed and transferred to cold storage. After expedition, all cores were transported under a cold condition (4°C) to the Kochi Core Center (KCC) in Kochi, Japan. The personal sampling party of each leg is planned at the KCC sometime after the core transportation.

Table 1. Hole summary of C9036.

Site	Hole	Location	Water depth (mbsl)	Number of Cores	Total Cored Interval (m)	Initial Recovery (%)
C9036	A	30° 51.2000' N, 130° 27.0000' E	233.0	2	0.5	0.0
	B	30° 51.2019' N, 130° 26.9978' E	233.0	14	32.5	109.3
	C	30° 51.2096' N, 130° 26.9889' E	233.0	1	2.0	119.0
	D	30° 51.2134' N, 130° 26.9845' E	233.0	1	4.5	84.4
	E	30° 51.2172' N, 130° 26.9800' E	233.0	2	9.0	90.9
	F	30° 51.2210' N, 130° 26.9756' E	233.5	1	4.5	96.2

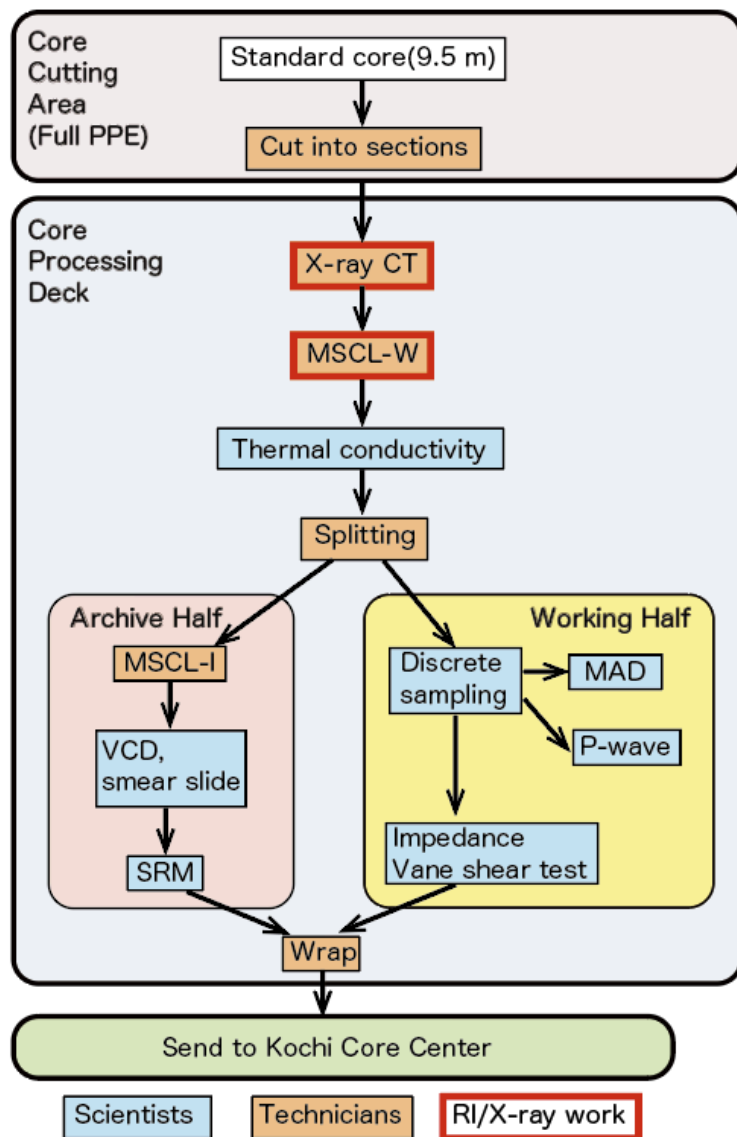


Fig. 4 Schematic illustration of shipboard core analysis flow.

7. Operation

The specific operation timetable for this expedition is described in **8. Cruise Log**.

The *Chikyu* SCORE Expedition 912 Leg.2 began at 2:00 on 8th January, 2020 when the vessel left the Leg.1 drill site (Enshu-nada). After transit, we arrived at the drill site on 10th January and started making up and running the Hydraulic Piston Coring System (HPCS) assembly without Guide Horn after confirming the low sea current. Spud-in occurred at 16:48 on 10th January at C9036A. Two cores were retrieved at the hole. However, since we had no recovery from both cores (Table 2), we moved the vessel to Hole B and shot for Core 1H on 21:00. Since the advance of Core 1H was very low, we then switched the coring system to S-HPCS.

On 11th and 12th January, we continued S-HPCS/HPCS coring and retrieved Cores 2F~14F. After

running inner barrel for Core 15F, high-torque and high weight on bit were observed, indicating that the hole condition was getting worse. Thus, we decided to abandon the hole and to try again the shallower part. The total depth of C9036B was 95 mbsf. We changed the location to Hole C (20 m northwestward from Hole B) and then Hole D (10 m northwestward from Hole C), and took one core from each hole. We changed the location again to Hole E, where 10 m NW from Hole D and retrieved Cores 1F and 2F. After the 2F coring, the hole condition got worse thus we decided to open a new hole, Hole F. With taking Core 1F from Hole F, we terminated the coring operations of this expedition. The vessel departed the drilling site on 13th January and arrived off the Port of Sasebo on 14th January. The expedition finished with docking of the vessel on 15th January.

Table 2. Summary of each core 's advance and recovery.

Recovery of all cores includes a fill (fall-in) portion at the top part.

Hole	Core	Below Seafloor (mbsf)		Advanced (m)	Recovery (m)	Recovery (%)
		Top of Core	Bottom of Core			
A	1H	0.0	0.5	0.5	0.00	0.0
A	2H	0.0	0.0	–	0.00	0.0
B	1H	3.0	3.5	0.5	0.53	106.0
B	2F	17.5	21.0	3.5	3.74	106.9
B	3F	21.0	25.0	4.0	4.40	110.4
B	4F	25.0	28.5	3.5	4.40	125.7
B	5H	28.5	33.5	5.0	5.34	106.8
B	6H	33.5	33.5	0.0	0.23	0.0
B	7F	33.5	33.5	0.0	0.63	0.0
B	8F	38.5	42.5	4.0	4.22	105.5
B	9F	42.5	43.0	0.5	0.60	120.0
B	10F	47.5	52.0	4.5	4.18	129.0
B	11F	52.0	52.0	0.0	0.00	0.0
B	12F	62.0	64.0	2.0	1.88	94.0
B	13F	74.0	78.5	4.5	4.33	96.2
B	14F	94.5	95.0	0.5	0.28	56.0
C	1F	10.0	12.0	2.0	2.38	119.0
D	1F	13.0	17.5	4.5	3.80	84.4
E	1F	16.0	20.5	4.5	3.95	87.7
E	2F	20.5	25.0	4.5	4.23	94.0
F	1F	18.9	22.5	4.5	4.33	96.2

8. Cruise Log

Date	Area	Plan
5th	Depart Shimizu port	Leave port
Jan	Start of Leg1	Transit
6th	Leg1(Enshu-Nada)	HPCS operation
7th	Leg1(Enshu-Nada)	HPCS operation
8th	00:00-02:30 POOH HPCS 02:30 Bit on deck 02:00-24:00 Sail to Leg2 site	End of Leg1 and move to Kikai site: Start of Leg 2
9th	00:00-24:00 Sail to Leg2 site	transit
10th	00:00-12:00 Sail to Leg2 site 12:00-14:10 DP setting 13:50-15:40 M/U and RIH HPCS BHA to 246 mBRT 16:30 Run HPCS inner barrel 16:48 Shoot Core 1H @252.5 mBRT 16:48-16:57 Release Core 1H w/CLW 16:57 Core 1H on deck, empty core 17:15-18:45 Replace core catcher and reset CLW length 18:33 Run HPCS inner barrel 18:48 Shoot Core 2H@259.5 mBRT 18:48-18:52 Release Core 2H w/CLW 18:53-19:01 Retrieve Core 2H 19:02 Core 2H on deck Move to Hole B because of no getting core 20:13 Run HCPS inner barrel 20:25-20:40 Drill down 261.5-264.5 mBRT. 21:00 Shoot Core 1H @264.5 mBRT 21:01-21:05 Release Core 1H w/CLW 21:05-21:13 Retrieve Core 1H 21:13 Core 1H on deck 21:45-22:30 Drop center bit 22:30-24:00 Drill down, 265.0-279.0 mBRT and bottoms up.	Transit/ HPCS
11th	00:00-00:30 Drill down (10 rpm, 50 spm), 265.0-279.0 mBRT and bottoms up. 00:30-01:15 Retrieve center bit 01:15 Run 2F S-HCPS Core inner barrel	HPCS

<p>02:41-02:58 Run 2F S-HCPS inner barrel</p> <p>03:00 Shoot Core 2F @278.0 mBRT (1m off bottom)</p> <p>03:03 Release Core 2F w/CLW and DW</p> <p>03:03-03:12 Retrieve Core 2F</p> <p>03:12 Core 2F on deck</p> <p>05:43 Run 3F S-HCPS Core inner barrel</p> <p>06:11 Shoot Core3F @282.0 mBRT (0.5m off bottom)</p> <p>06:12 Release Core 3F w/DW</p> <p>06:12-06:22 Retrieve Core 3F</p> <p>06:22 Core 3F on deck</p> <p>06:25 Run 4F S-HCPS Core inner barrel, Drill down to 286.5 mBRT</p> <p>07:18 Shoot Core 4F @285.5 mBRT (1.0m off bottom)</p> <p>07:23 Release Core 4Fw/DW</p> <p>07:23-07:30 Retrieve Core 4F</p> <p>07:30 Core 4F on deck</p> <p>07:56 Run 5H HCPS Core inner barrel, Drill down to 290.0 mBRT</p> <p>08:23 Shoot Core 5H @289.0 mBRT (1.0m off bottom)</p> <p>08:30 Release Core 5H w/DW (No overpull)</p> <p>08:30-08:45 Retrieve Core 5H</p> <p>07:45 Core 5H on deck</p> <p>09:09 Run 6H HCPS Core inner barrel, Drill down to 295.0 mBRT</p> <p>09:39 Shoot Core 6H @294.0 mBRT (1.0m off bottom)</p> <p>09:41 Release Core 6H w/CLW</p> <p>09:41-09:49 Retrieve Core 6H</p> <p>09:49 Core 6H on deck</p> <p>10:20 Run 7F S-HCPS Core inner barrel</p> <p>10:40 Shoot Core @295.0 mBRT on bottom</p> <p>10:41 Release Core 7F w/CLW</p> <p>10:41-10:51 Retrieve Core 7F</p> <p>10:51 Core 7F on deck</p> <p>11:00-13:30 Unload sinker bar, Drop center bit, Drill down 10m, Sweep, recover center bit</p> <p>13:30 Run 8F S-HCPS Core inner barrel</p>	
---	--

	<p>13:49 Shoot Core 8F @295.0 mBRT on bottom 13:49-13:52 Release Core 8F w/CLW 13:52-14:02 Retrieve Core 8F 14:02 Core 8F on deck 15:04 Run 9F S-HCPS Core inner barrel 15:23 Shoot Core 9F @304.0 mBRT on bottom 15:23-15:25 Release Core 9F w/CLW and DW 15:25-15:35 Retrieve Core 9F 15:35 Core on deck 16:00-17:55 Unload sinker bar, Drop center bit, Drill down 10m, Sweep, recover center bit 17:57 Run 10F S-HCPS Core inner barrel 18:21 Shoot Core 10F @309.0 mBRT on bottom 18:21-18:23 Release Core 10F w/CLW and DW 18:23-18:35 Retrieve Core 10F 18:35 Core 10F on deck 20:30 Run 11F S-HCPS Core inner barrel 20:48 Shoot Core 11F @313.5 mBRT on bottom 20:48-20:51 Release Core 11F w/CLW and DW 20:51-21:05 Retrieve Core 11F 21:05 Core 11F on deck 22:12-23:50 Unload sinker bar, Drop center bit, Drill down 10m, Sweep, recover center bit 23:52 Run 12F S-HCPS Core inner barrel</p>	
12th	<p>00:00 Cont. Run 12F S-HCPS Core inner barrel 00:08 Shoot Core 12F @323.5 mBRT on bottom 00:11 Release Core w/CLW and DW 00.11-00:21 Retrieve Core 12F 00:21 Core 12F on deck 00:30- 02:23 Unload sinker bar, Drop center bit, Drill down 10m, Sweep, recover center bit 02:24 Run 13F S-HCPS Core inner barrel 02:46 Shoot Core 13F @335.5 mBRT on bottom 02:47 Release Core 13F w/CLW and DW 02.47-03:04 Retrieve Core 13F 03:04 Core 13F on deck</p>	HPCS

<p>03:15- 06:55 Unload sinker bar, Drop center bit, Drill down 16m, Sweep, recover center bit</p> <p>06:55 Run 14F S-HCPS Core inner barrel</p> <p>07:23 Shoot Core 14F @356.0 mBRT on bottom</p> <p>07:23 Release Core w/CLW and DW</p> <p>07.23-07:37 Retrieve Core 14F</p> <p>07:37 Core 14F on deck</p> <p>08:40 Run 15F S-HCPS Core inner barrel</p> <p>After running inner barrel, string was stalled observing high-Trq and high-WOB. It was decided to abandon hole and move to next hole.</p> <p>10:00-13:20 Move vessel (20 m NW from Hole B), Drop center bit, Spud-in Hole C, Drill down to 271.5 mBRT, Retrieve center bit</p> <p>13:20 Run 1F S-HCPS Core inner barrel</p> <p>13:39 Shoot Core 1F @271.5 mBRT on bottom</p> <p>13:41 Release Core 1F w/CLW and DW</p> <p>13.41-13:49 Retrieve Core 1F</p> <p>13:49 Core 1F on deck</p> <p>14:20-16:20 Move vessel (10 m NW from Hole C), Drop center bit, Spud-in Hole D, Drill down to 274.5 mBRT, Retrieve center bit</p> <p>16:23 Run 1F S-HCPS Core inner barrel</p> <p>16:46 Shoot Core 1F @274.5 mBRT on bottom</p> <p>16:47 Release Core 1F w/CLW</p> <p>16.47-16:56 Retrieve Core 1F</p> <p>16:56 Core 1F on deck</p> <p>17:20-20:05 Move vessel (10 m NW from Hole D), Drop center bit, Spud-in Hole E, Drill down to 277.5 mBRT, Retrieve center bit</p> <p>20:06 Run 1F S-HPCS Core inner barrel</p> <p>20:28 Shoot Core 1F @277.5 mBRT on bottom</p> <p>20:29 Release Core 1F w/CLW.</p> <p>20.29-20:40 Retrieve Core 1F</p> <p>20:40 Core 1F on deck</p> <p>21:56 Run 2F S-HPCS Core inner barrel</p>	
--	--

	22:29 Landing 22:30 Shoot Core 2F @282.0 mBRT on bottom 22:33 Release Core 2F w/CLW and DW 22.34-22:45 Retrieve Core 2F 22:46 Core 2F on deck 23:00-24:00 Move vessel (10 m NW from Hole E), Drop center bit, Spud-in Hole F, Drill down to 277.5 mBRT, Retrieve center bit	
13th	00:00-02:55 Move vessel (10 m NW from Hole E), Drop center bit, Spud-in Hole F, Drill down to 280.0 mBRT, Retrieve center bit 02:56 Run 1F S-HPCS Core inner barrel 03:15 Landing 03:17 Shoot Core 1F @323.5 mBRT on bottom 03:19 Release Core 1F w/CLW and DW 03.19-03:26 Retrieve Core 1F 03:27 Core 1F on deck 03:45-04:30 Return sinker bar and Service CLW 04:30-05:15 Unload sinker bar and flush inner string 05:15-06:45 POOH HPCS BHA 07:00-24:00 Sail to Sasebo	HPCS
14th	Arrived off port of Sasebo	Transit
15th	Docking of the vessel, end of cruise 12:30 disembarkation	End of cruise

9. Method and result of onboard research activities

9.1. X-ray computed tomography

X-ray CT images were done immediately after dividing the core into sections and were used to identify 3-D sedimentary and structural features, such as bioturbation burrows, bedding planes, faults, mineral veins, and so on. The X-ray CT images also performs the preliminary assessment of core quality through imaging destruction of geological features and drilling disturbance.

Method

Our methods followed those in the measurement manual prepared by Institute for Marine-Earth Exploration and Engineering (MarE3) (3D X-ray CT Scanning, Version 3.00; 24 March 2015). The X-ray CT instrument on the *Chikyu* is a Discovery CT 750HD (GE Medical Systems) capable of generating thirty-two 0.625 mm thick slice images every 0.4 s, the time for one revolution of the X-

ray source around the sample. Data generated for each core consist of core-axis-normal planes of X-ray attenuation values with dimensions of 512×512 pixels. Data were stored on the server as Digital Imaging and Communication in Medicine (DICOM) formatted files. The DICOM files were restructured to create 3-D images for further investigation.

The theory behind X-ray CT has been well established through medical research and is very briefly outlined here. X-ray intensity varies as a function of X-ray path length and the linear attenuation coefficient (LAC) of the target material:

$$I = I_0 \times e^{-\mu L},$$

where

I = transmitted X-ray intensity,

I_0 = initial X-ray intensity,

μ = LAC of the target material, and

L = X-ray path length through the material.

LAC is a physical index about the X-ray beam reduction during translation of target materials. LAC is led from the relationship between physical properties of target materials (i.e., chemical composition, density, and state). The basic measure of attenuation, or radiodensity, is the CT number given in Hounsfield units (HU):

$$\text{CT number} = [(\mu_t - \mu_w)/\mu_w] \times 1000,$$

where

μ_t = LAC for the target material, and

μ_w = LAC for water.

The distribution of attenuation values mapped to an individual slice comprises the raw data that are used for subsequent image processing. Successive 2-D slices yield a representation of attenuation values in 3-D pixels referred to as voxels. Analytical standards used during Expedition 370 were air (CT number = -1000), water (CT number = 0), and aluminum ($2477 < \text{CT number} < 2487$) in an acrylic core mock-up. All three standards were run once daily after air calibration. For each standard analysis, the CT number was determined for a 24.85 mm^2 area at fixed coordinates near the center of the cylinder.

Results

The X-ray CT instrument worked well enough to obtain X-ray CT images for our investigation. One example of the X-ray CT image is shown in Fig. 4.

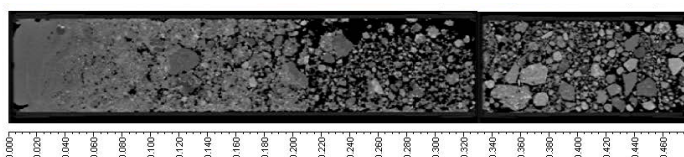


Fig. 4 An image of the X-ray CT of a Hole B core.

9.2. Physical properties measurements of whole-round core with the Multi-Sensor-Core-Logger

All physical property measurements were conducted after cores were thermally equilibrated at room temperature for approximately 4 hours. The MSCL-W (GeoTek Ltd., London, United Kingdom) allows nondestructive measurements on whole-round core (WRC) samples including gamma ray attenuation (GRA) density, ultrasonic P-wave velocity (VP), noncontact electrical resistivity (NCR), magnetic susceptibility (MS), and natural gamma radiation (NGR).

Method

Gamma ray attenuation (GRA) density: Bulk density is used to evaluate pore volume in sediment, which provides information on the consolidation state. GRA is based on the detection of a gamma ray beam during its passage through the sediment. The beam, produced by a 370 MBq ^{137}Cs gamma ray source within a lead shield with a 5 mm collimator, was directed through WRCs. The gamma ray detector includes a scintillator and an integral photomultiplier tube to record the gamma rays that pass through the WRC. GRA bulk density (ρ_b) was calculated as

$$\rho_b = \ln(I_0/I)/\mu d,$$

where

I_0 = gamma ray source intensity,

I = measured intensity of gamma rays passing through the sample,

μ = Compton attenuation coefficient, and

d = sample diameter.

The Compton attenuation coefficient (μ) and source intensity (I_0) were treated as constants, so ρ_b can be calculated from I . The gamma ray detector was calibrated with a sealed calibration core (a standard core liner filled with distilled water and aluminum cylinders of various diameters). To establish the calibration curves, gamma ray counts were measured through a 7 cm diameter standard cylinder composed of aluminum with six different diameters

(1–6 cm) (density = 2.7 g/cm³) filled with surrounding

relationship between I and μd is

$$\ln(I) = A(\mu d) + B,$$

where A and B are coefficients determined from the calibration experiment. GRA density measurements on core samples were conducted every 2 cm for 4 s. The spatial resolution is 5 mm.

Ultrasonic P-wave velocity: Ultrasonic P-wave velocity (VP) was measured for WR cores by measuring sonde length (d) (outer liner diameter) and travel time (t_0):

$$VP = d/t_0.$$

A linear variable differential transformer, used to measure the liner thickness, is integrated

with a 230 kHz P-wave transmitter/receiver system. The system is mounted horizontally on the MSCL-W system and measures d and t_0 perpendicular to the core axis at 2 cm intervals. The measured travel time (t_0) between the transducers is delayed by the pulse travel time through the liner, the threshold peak detection procedure, and the pulse travel between transducers and the electronic circuitry. Travel time is corrected for these parameters by calibrating the system using a core liner filled with pure water, which has a known P-wave velocity (1480 m/s at 20°C). The corrected P-wave velocity through the core (V_{core}) (m/s) is

$$V_{\text{core}} = (d - W) / [t_0 - t_w - (d - W) / V_w],$$

where

W = total wall thickness of the core liner,

t_w = measured travel time through the water-filled calibration liner, and

V_w = known P-wave velocity of pure water at room temperature.

Noncontact electrical resistivity (NCR): Within limits, electrical resistivity may be useful for estimating other sediment physical properties, including porosity, tortuosity, permeability, and thermal conductivity. Bulk electrical resistivity is controlled by solid grain resistivity, interstitial water resistivity, pore space distribution, and pore connectivity. Electrical resistivity (ρ) is defined by the electrical resistance and geometry of the core measured:

$$\rho = R(A/L)$$

where R = electrical resistance, L = length of measurement, and A = cross-sectional area of the core.

The noncontact resistivity sensor on the MSCL-W system induces a high-frequency magnetic field in the core with a transmitter coil. This generates an electrical current in the bulk sediment that is inversely proportional to its resistivity. The secondary magnetic field generated by this induced electrical current is measured by a receiver coil. To measure this smaller magnetic field accurately, a differencing technique has been developed that compares readings from the sample core to readings from an identical set of coils operating in air. Electrical resistivity data were obtained at 2 cm intervals on the MSCL-W.

Magnetic susceptibility (MS): MS is the degree to which a material can be magnetized by an external magnetic field. Therefore, MS reflects the composition of sediment. An 8 cm diameter Bartington loop sensor was used to measure MS. An oscillator circuit in the sensor produces a low-intensity (~80 A/m root-mean-square) nonsaturating alternating magnetic field (0.565 kHz). This pulse frequency was converted into MS. The spatial resolution of the loop sensor is 23–27 mm. MS data were collected every 2 cm along the core.

Natural gamma radiation (NGR): NGR measurements provide insights into sediment composition

and thus can be used to identify lithology. WRCs are monitored for NGR emissions to obtain spatial variability in radioactivity. NGR measurement employs lead-shielded counters optically coupled to a photomultiplier tube and connected to a bias base that supplies high-voltage power and a signal preamplifier. Two horizontal and two vertical sensors are mounted in a lead cube-shaped housing. The NGR system records radioactive decay of ^{40}K , ^{232}Th , and ^{238}U and has a resolution of 120–170 mm in terms of core length. Measurements were conducted every 16 cm with a count time of 30 s. Background radiation noise was determined by taking measurements on a water-filled calibration core. Two radioactive isotope standards (^{133}Ba and ^{60}Co) were used for energy calibration and adjustment of the spectral detection windows.

Results

Physical properties (GRA, VP, NCR, MS, and NGR) measured by the MSCL-W instrument were properly obtained.

9.3. Physical properties except for the MSCL-W measurement

Thermal conductivity was measured on whole-round core samples. Shear strength test, impedance measurement and MAD discrete sampling were routinely carried out for working-half cores. Moisture and density (MAD) were measured on discrete samples collected from working-half cores. MAD analyses provide information on water content, bulk density, porosity, void ratio, and grain density. P-wave velocity and electrical resistivity measurements were taken on discrete cube samples in the x-, y-, and z-directions to evaluate anisotropy of velocity and resistivity. Details and procedures for each measurement are described below.

Method

Thermal conductivity measurements: Thermal conductivity measurements were conducted using two thermal conductivity measuring system (TK04 system) (Blum, 1997) on whole-round core samples (Von Herzen and Maxwell, 1959; Vacquier, 1985). A small hole was drilled at measuring point of the core liner in order to insert the needle probe and a needle probe of 2 mm in diameter was inserted. All thermal conductivity measurements were made after the cores had equilibrated to room temperature (> three hours of waiting time at the core processing deck). A section was placed in a thermal insulation box to stabilize air temperature during the measurement. At the beginning of each measurement, temperature in the sediment was monitored to ensure that thermal drift becomes small enough (typically within a couple of minutes). After it was established that the temperature was near equilibrium, a calibrated linear heat (2.5 W/m) was applied, and the rise in temperature was recorded for 80 seconds. Values of thermal conductivity were calculated based on the observed rise in temperature for a given quantity of heat. Each thermal conductivity measurement was performed

repeatedly five times, and the arithmetic mean was calculated as a representative value.

Empirical tests to check system condition or performances were conducted with a certified MACOR ceramic standard sample ($k = 1.623 \text{ W}/[\text{m}\cdot\text{K}] \pm 2\%$). $3.5 \text{ W}/\text{m}$ of heat power was applied for the standard sample measurement. The empirical tests were performed at least once a day.

Shear strength measurements: Undrained shear strength were measured using a semi-automated laboratory vane shear device (Model WF23500) and a penetrometer (Model E-284B).

Vane shear measurements were made with the vane rotation axis at a frequency of one to five (generally two) per core. The vane shear strength of sediments $S_u(v)$ (kPa) is calculated as:

$$S_u(v) = T / K_v,$$

where T (N-m) is the torque required to fail the material and K_v (m^3) is a constant depending on the dimensions of the vane (Blum, 1997). All measurements reported here were obtained using a vane with height and diameter equal to 12.7 mm. Failure torque was determined by measuring the degrees of rotation of a spring (Spring-1 used onboard the *Chikyu*) and a linear calibration equation (manufacturer specified) relating the rotation angle to torque for the particular spring being used. Vane shear results were generally considered reliable for shear strength values less than approximately 150 to 200 kPa, above which excessive cracking and separation of the core material occurred.

The penetrometer provides a measure of unconfined compressive strength (UCS) of sediment samples. The UCS is calculated by dividing the penetration resistance generated by pushing a cylindrical probe into the core surface to a 6.5 mm penetration depth by the area of the penetration probe (Blum, 1997). All measurements in this expedition were conducted using a probe with a nominal diameter of 6.35 mm (0.25 inches). The UCS values were calculated from the average of three penetration trials conducted at adjacent points on the core. Typical spatial separation between trials was on the order of 1 cm. The unit was converted from kg/cm^2 to kPa by the following equation as,

$$\text{UCS (kPa)} = \text{UCS (kg}/\text{cm}^2) * 9.81 * 10.$$

The undrained shear strength $S_u(v)$ (kPa) is calculated by dividing the measured UCS (kPa) by 2.

Moisture and density measurements: Index properties (bulk density, grain density, water content, porosity, and void ratio) of core samples were calculated from measurements of wet masses, dry masses, and dry volumes on discrete samples. Basically, $\sim 10 \text{ cm}^3$ of sediment was sampled by a plastic syringe (20 mm in diameter).

Wet and dry masses were measured using a paired electronic balance system designed to compensate for the ship's heave. The sample mass was counterbalanced with a precisely known mass (40 g) that was suitable for 30–50 g sample mass measurements. The sample mass was determined to a precision of $\pm 0.01 \text{ g}$. The balance system was calibrated every day. Immediately after the samples were collected, wet sediment mass was measured. Dry sediment mass and volume were measured after drying the

samples in a convection oven for 24 h at $105^\circ \pm 5^\circ\text{C}$. Dried samples were then cooled in a dry desiccator for 1 h before the measurement of dry mass. Dry volume was measured by using a helium-displacement five-cell pycnometer with a nominal precision of $\pm 0.04 \text{ cm}^3$. Cell volumes were calibrated every day. A reference volume (calibrated sphere) was run with each set of four samples, and the sphere was rotated in the cells in order to check any systematic error. For calculation of bulk wet and dry density, grain density, porosity, and void ratio, the traditional ODP method is used (Method C in Blum, 1997). Water content, porosity, and void ratio are defined by the mass or volume of extracted water before and after removal of interstitial water through the drying process. Standard seawater density (1.024 g/cm^3) was assumed for the density of interstitial water calculation.

Impedance measurements: Electrical impedance as a complex quantity (magnitude $[|Z|]$ and phase $[\theta]$) was measured with a precision impedance analyzer (Agilent 4294A) using the bridge method. Two techniques were used for measurement; a four-pin-electrode array (16089D alligator clip leads) for target points in a working half samples and two electrodes for cubic samples ($\sim 2 \text{ cm} \times 2 \text{ cm} \times 2 \text{ cm}$) (16451B test fixture).

Complex impedances at target points in working half cores were measured with a four-pin array consisting of four electrodes spaced 7.5 mm apart. The electrode array was inserted along the y-direction of the working half. Measurements were conducted using AC current over a wide range of frequency (40 Hz - 100 kHz). The final data were selected at measurement values at 25 kHz.

Complex impedances for cubic samples, which were saturated with 35 g/L NaCl solution in advance, were measured between two stainless steel electrodes covered with seawater-saturated filters. Measurements for each cubic sample were conducted three times in three directions (x-, y-, and z-directions) of the coordinate system for the sample, which was same as the coordinate system for the original working half (core reference frame). The final data for each measurement was selected at 25 kHz in the same manner as the above pin-electrode-array method. Three-directional data, together with dimensions of the sample, are used to derive horizontal and vertical electrical anisotropies.

Room temperature in the laboratory was also recorded at the time of each measurement. The temperature data are used for accounting for temperature variations, which affect impedance measurement.

Fixture compensation was conducted to reduce the effect of the error sources between the sample and the instrument. Two types of the compensation (OPEN and SHORT) were performed after turning on the instrument and once a day.

Electrode cell constant was obtained by measuring the standard seawater (IAPSO P-series, S=35), which was required to calculate electrical resistivity of the sample. Formation Factor is calculated from the resistivity of the sample and the standard seawater.

P-wave velocity measurements: Discrete P-wave velocity was measured with the P-wave logger (PWV-D) on cubic samples (~2 cm × 2 cm × 2 cm) cut from working half samples. The oriented cubic samples were soaked in 35% NaCl solution and rotated manually to measure x-, y-, and z-axis velocities. The P-wave logger is equipped with two 230 kHz transducers, one used as a transmitter and one as a receiver. Sample length (L) was measured with a laser distance sensor. The P-wave velocity in any direction (e.g., VPx) was calculated from the sample length (e.g., Lx), total traveltime (tx), and system-calibrated delay time (tdelay):

$$VPx = Lx / (tx - tdelay).$$

Horizontal anisotropy of velocity (Avh) and vertical anisotropy of velocity (Avv) were calculated using the following equations:

$$Avh = 200[(VPx - VPy)/(VPx + VPy)], \text{ and}$$

$$Avv = 200[(VPx + VPy)/2 - VPz] / [(VPx + VPy)/2 + VPz],$$

where VPx, VPy, and VPz are the velocity in each axial direction.

Routine QC measurements were performed every 24 h by measuring velocity on glass and acrylic standards with known lengths and velocities.

Results

Thermal conductivity measurements: The measurement frequency was about two points per section. Measuring points are summarized in Table 3. Almost all measurements were conducted without significant technical problems and valuable data was obtained.

Table 3. Measurement list of thermal conductivity

Test point	Depth (mbsf)
Hole B	
C9036B-2F2-129 cm	19.435
C9036B-2F3-88 cm	20.319
C9036B-3F2-72 cm	22.962
C9036B-3F4-7 cm	24.227
C9036B-4F2-7.5 cm	26.184
C9036B-5H2-7 cm	29.526
C9036B-5H4-7 cm	32.217
C9036B-8F1-94 cm	39.44
C9036B-8F2-70 cm	40.504
C9036B-10F2-70.5 cm	48.57
C9036B-10F4-63 cm	51.23
C9036B-12F2-68 cm	63.167

(Table 3 continued)

C9036B-13F2-67 cm	75.79
C9036B-13F4-17 cm	77.835
Hole D	
C9036D-1F2-24 cm	14.44
C9036D-1F3-65 cm	16.455
Hole E	
C9036E-1F2-101 cm	18.41
C9036E-1F3-82 cm	19.52
C9036E-2F1-123 cm	21.73
C9036E-2F3-38 cm	23.71
Hole F	
C9036F-1F2-10 cm	19.29
C9036F-1F2-48 cm	19.67

Shear strength measurements: Vane shear measurements were made at discrete about two locations per section on the working half samples. In general, measurements were made adjacent to MAD sampling locations. Care was taken to conduct tests within undisturbed and homogeneous parts of the core. To minimize disturbance effects resulting from the MAD sampling, shear measurements were generally conducted first, followed by MAD sampling. The penetrometer measurements were made at two locations on Hole C9036B and C9036D. Measuring points are summarized in Table 4. Almost all measurements were conducted without significant technical problems and valuable data was obtained.

Table 4. Measurement list of vane shear strength.

Test point	Depth (mbsf)
Hole B	
C9036B-3F2-30 cm	22.542
C9036B-3F3-69 cm	23.881
C9036B-4F2-42 cm	26.529
C9036B-4F3-126 cm	28.497
C9036B-5H3-83 cm	31.671
C9036B-5H4-36.5 cm	32.512
C9036B-8F1-105 cm	39.55
C9036B-8F3-72 cm	41.846
C9036B-10F2-101 cm	48.875

(Table 4 continued)

C9036B-10F3-26.5 cm	49.45
C9036B-12F3-14.5 cm	63.304
C9036B-12F3-79.5 cm	63.954
C9036B-13F1-105 cm	75.05
C9036B-13F2-67 cm	75.79
C9036B-13F3-54 cm	77.005

Hole C

C9036C-1F2-73 cm	11.745
------------------	--------

Hole D

C9036D-1F3-69 cm	16.495
C9036D-1F3-79 cm	16.595
C9036D-1F3-81 cm	16.615

Hole E

C9036E-1F3-50 cm	19.2
C9036E-1F3-60 cm	19.3
C9036E-1F3-67 cm	19.37
C9036E-2F1-67 cm	21.17
C9036E-2F3-84 cm	24.17

Hole F

C9036-1F1-60 cm	18.6
C9036-1F1-64 cm	18.64
C9036-1F1-68 cm	18.68
C9036-1F2-91 cm	20.1
C9036-1F4-31 cm	21.92

Moisture and density measurements: MAD samples was collected from about two intervals of each section for working half samples. Each discrete sample for MAD were collected from the surface of the section avoiding the core disturbance caused by the strength tests and impedance measurement. Sampling points are summarized in Table 5. Almost all measurements were conducted without significant technical problems and valuable data was obtained.

Table 5. Measurement list of MAD.

Test point (top)	Depth (mbsf)
Hole B	
C9036B-3F2-24cm	22.482
C9036B-3F3-63cm	23.821
C9036B-4F2-36cm	26.469
C9036B-4F3-120cm	28.437
C9036B-5H3-77cm	31.61
C9036B-5H4-30cm	32.447
C9036B-8F1-100cm	39.5
C9036B-8F3-67cm	41.796
C9036B-10F2-100cm	48.865
C9036B-10F3-25cm	49.44
C9036B-12F3-14cm	63.299
C9036B-12F3-74cm	63.899
C9036B-13F1-40cm	74.4
C9036B-13F1-104cm	75.04
C9036B-13F2-66cm	75.78
C9036B-13F3-53cm	76.995
C9036B-13F3-63cm	77.095
C9036B-13F3-82cm	77.285
C9036B-14Fcc-22cm	94.72
Hole C	
C9036C-1F2-71cm	11.725
Hole D	
C9036D-1F3-68cm	16.485
C9036D-1F3-80cm	16.605
Hole E	
C9036E-1F2-58cm	17.98
C9036E-1F2-103cm	18.43
C9036E-2F1-80cm	21.3
C9036E-2F3-70cm	24.03
Hole F	
C9036F-1F1-115cm	19.15
C9036F-1F3-20cm	20.8

Impedance measurements: Impedance measurements using a four-pin-electrode array and two electrodes was conducted at about two points of each section for working half samples and three cubic samples, respectively. Measuring points are summarized in Table 6. Almost all measurements were conducted without significant technical problems and valuable data was obtained.

Table 6. Measurement list of impedance

Test point	Depth (mbsf)
Hole B	
C9036B-3F2-27 cm	22.512
C9036B-3F3-67 cm	23.861
C9036B-4F2-40 cm	26.509
C9036B-4F3-124 cm	28.477
C9036B-5H3-81 cm	31.651
C9036B-5F4-34 cm	32.487
C9036B-8F1-104 cm	39.54
C9036B-8F3-70 cm	41.826
C9036B-10F2-99 cm	48.855
C9036B-10F3-25 cm	49.44
C9036B-12F3-13 cm	63.289
C9036B-12F3-75.5 cm	63.914
C9036B-13F1-105.5 cm	75.055
C9036B-13F2-66 cm	75.78
C9036B-13F3-53 cm	76.995
Hole C	
C9036C-1F2-72 cm	11.735
Hole D	
C9036D-1F3-68 cm	16.485
C9036D-1F3-79 cm	16.595
Hole E	
C9036E-1F3-50.5 cm	19.205
C9036E-1F3-64 cm	19.34
C9036E-1F3-68.5 cm	19.385
C9036E-2F1-63 cm	21.13
C9036E-2F1-68 cm	21.18
C9036E-2F3-84 cm	24.17

(Table 6 continued)

Hole F

C9036F-1F1-60 cm	18.6
C9036F-1F1-65 cm	18.65
C9036F-1F1-70 cm	18.7
C9036F-1F1-76 cm	18.76
C9036F-1F2-62 cm	19.81
C9036F-1F2-65 cm	19.84
C9036F-1F2-91 cm	20.1
C9036F-1F4-31 cm	21.92

P-wave velocity measurements: P-wave velocity of cubic samples used by the impedance measurement were measured. Sampling points are plotted in Table 7. Measurements were conducted without significant technical problems and valuable data was obtained.

Table 7. Measurement list of P-wave velocity

Test point	Depth (mbsf)
Hole B	
C9036B-13F1-40 cm	74.4
C9036B-13F3-63 cm	77.095
C9036B-14FCC-22 cm	94.72

Residues of the samples for these physical properties were recovered and used for petrological observation as personal samples.

9.4. Lithology

We observed cut surface of the core sections to describe lithology and identify sedimentary units.

Method

After the MSCL-W and thermal conductivity measurement, all the core sections were split into two parts, archive halves and working halves, in the *Chikyu* from January 11th to 14th. The cut surface image of the archive half was recorded using MCLS-I machine. Then, visual core description of the archive half was carried out. Each sediment unit was identified based on rock type, size, shape, vesicularity, and color of particles in the sediments.

Results

The thicknesses of cored sediments were 0.0 m at Hole C9036A, 32.5 m at Hole C9036B, 2.0 m at Hole C9036C, 4.5 m at Hole C9036D, 9.0 m at Hole C9036E, and 4.5 m at Hole C9036F.

The recovered sediment was not consolidated. Bioturbation was not observed.

C9036A: There was no recovery of sediments at Hole C9036A.

C9036B: Main units of the cores were two units of volcanoclastic deposit and a unit of sandy silt between them. Upper volcanoclastic deposit mainly consisted of slightly reddish to orange pumice lapilli and ash. The recovered thickness of this volcanoclastic deposit is about 2.4 m. The underlying sandy silt consists of very fine fragments of black volcanic rock. It contains small fragments (~ 5 mm) of sea shell and other organic material. Some foraminifer were also observed. The recovered thickness of the sandy silt is about 12.6 m. The sandy silt underlain by the lower volcanoclastic deposit. This volcanoclastic deposit mainly consisted of white pumice lapilli and ash, which characteristically contain quartz. The recovered thickness of this volcanoclastic deposit is about 17 m.

C9036C: Main lithology of the cores was lapilli of dark, gray, white, and reddish volcanic rocks. Some normally graded units can be recognized. The recovered thickness of this sediment was about 1.5 m. A unit of about 10 cm thick muddy stratified sediment was also observed between two lapilli units.

C9036D: Main units of the cores were two units of volcanoclastic deposit. The upper unit mainly consisted of ill-sorted lapilli of pumice, obsidian, and dark, white, reddish, and pale green volcanic rocks. The recovered thickness of this volcanoclastic deposit was about 3.2 m. The lower volcanoclastic deposit mainly consisted of slightly reddish to orange ash. The recovered thickness of this volcanoclastic deposit was about 0.5 m.

C9036E: Main units of the cores were two units of volcanoclastic deposits and an underlying sandy silt unit. The upper volcanoclastic deposit mainly consists of white to light gray pumice and dark gray volcanic rock. The recovered thickness of this volcanoclastic deposit was about 1.3 m. The lower volcanoclastic deposit mainly consisted of slightly reddish to orange fine pumice lapilli and ash. The recovered thickness of this volcanoclastic deposit was about 2.5 m. The sandy silt unit consists of very fine fragments of black volcanic rock. It contains small fragments (~ 5 mm) of sea shell and other organic material. Some foraminifer were also observed. The recovered thickness of the sandy silt is about 4.1 m.

C9036F: Main units of the cores were a unit of volcanoclastic deposit and a unit of sandy silt. The volcanoclastic deposit mainly consisted of slightly reddish to orange pumice lapilli and ash. The recovered thickness of this volcanoclastic deposit was about 1.2 m. The sandy silt unit consists of very fine fragments of black volcanic rock. It contains small fragments (~ 5 mm) of sea shell and other organic material. Some foraminifer were also observed. The recovered thickness of the sandy silt is about 2.8 m.

We sampled shells at the interval of 85.5, 91, and 98 cm from the top of the section 2, Core 3F, C9036B for ¹⁴C dating.

9.5. Paleomagnetism

Paleomagnetic and rock magnetic investigations were conducted to determine the characteristic of remanence directions for use in magnetostratigraphic and structural studies. Archive halves were measured with the superconducting rock magnetometer (SRM).

Method

The paleomagnetism laboratory on board the *Chikyu* houses a large (7.3 m × 2.8 m × 1.9 m) magnetically shielded room, with its long axis parallel to the ship transverse. The total magnetic field inside the room is ~1% of Earth's magnetic field. The room is large enough to comfortably handle standard IODP core sections (~1.5 m). The long-core SRM is a liquid helium free cooling system (4K SRM: WSGI); the 4K SRM uses a Cryomech pulse tube cryocooler to achieve the required 4 K operating temperatures without the use of any liquid helium. The differences between the pulse tube cooled system and the liquid helium cooled magnetometers have very significant impact on the system ease of use, convenience, safety and long-term reliability. The SRM system is ~6 m long with an 8.1 cm diameter access bore. A 1.5 m split core liner can pass through a magnetometer, an alternating-field (AF) demagnetizer, and an anhysteretic remanent magnetizer. The system includes three sets of superconducting pickup coils, two for transverse moment measurement (x- and y-axes), and one for axial moment measurement (z- axis). The noise level of the magnetometer is $<10^{-7}$ A/m for a 10 cm³ volume rock. An automated sample handler system (2G804) included in the magnetometer consists of aluminum and fiberglass channels and designated to support and guide long core movement. The core itself is positioned in a nonmagnetic fiberglass carriage that is pulled through the channels by a rope attached to a geared high-torque stepper motor. A 2G600 sample degaussing system is coupled to the SRM to allow automatic demagnetization of samples up to 100 mT. The system is controlled by an external computer and enables programming of a complete sequence of measurements and degauss cycles without removing the long core from the holder.

Remanent magnetizations of all the archive-half sections from Holes C9036 A to F were measured at demagnetization levels of 0, 10, and 20 mT peak fields in order to recognize stable magnetic components. It is confirmed that low-coercivity components can be removed by demagnetizations step of 10 mT.

10. Post-cruise study plan

The aims of our study on Kikai caldera volcano are volume estimation and understanding of magmatic features of the CCFEs. After the expedition 912 cruise, we plan investigations in the following.

(1) Change of whole-rock composition of volcanic ejecta through eruption in the two CCFEs.

Information of compositional change of magma with the progress of eruption is important to know configuration of the magma chamber. In order to elucidate it, vertical changes of whole-rock

composition of the volcanic ejecta in the two Kikai CCFEs will be analyzed with JSX-3600CAZ TATSCAN-F2 in Kochi Core Center.

(2) Personal sampling and analyses on petrology and geochemistry

We will collect representative samples of volcanic ejecta and marine sediments throughout the cores from their working halves, and obtain petrological data of them as follows:

Petrography with microscope,

Whole-rock composition (major and minor elements and isotope),

Volcanic glass (shards) composition,

Composition of phenocryst crystals.

(3) Reconsidering stratification and estimation of eruption volumes

We will reconsider correlation among the strata in the cores, the layers obtained in the multi-channel seismic reflection survey, and the eruption events recognized in the subaerial geological studies based on the above petrological features and sedimentary structures. Correlation between an eruption event and a layer by seismological study allow us to evaluate spatial distribution and thickness of the layer by the eruption and estimate eruption volume.

11. References

- Blum, P., 1997. Physical properties handbook: a guide to the shipboard measurement of physical properties of deep-sea cores. ODP Tech. Note, 26.
- Machida, H., Ōta, Kawana, T., Moriwaki, H., Nagaoka, S., 2001. Geomorphology of Japan 7 Kyushu–Nansei syotou. University of Tokyo Press. 355 pp. (in Japanese).
- Maeno, F. and Taniguchi, H., 2007. Spatiotemporal evolution of a marine caldera-forming eruption, generating a low-aspect ratio pyroclastic flow, 7.3 ka, Kikai caldera, Japan: Implication from near-vent eruptive deposits. *Journal of Volcanology and Geothermal Research*, 167, 212-238.
- Matsushita, M., 2002. Vegetation Changes under the Influence of the Kikai-Akahoya Eruption in Osumi Peninsula, Southern Kyushu, Japan. *The Quaternary Research*, 41, 301-310.
- Ono, K., T. Soya, and T. Hosono, 1982. Geology of the Satsuma-Io-jima district, Quadrangle series, scale 1:50000, Geological Survey of Japan. 80 p., (in Japanese with English abstract).
- Tatsumi, Y. and Suzuki-Kamata, K., 2014. Cause and risk of catastrophic eruptions in the Japanese Archipelago. *Proceedings of the Japan Academy*, 20, 347-352.
- Tatsumi, Y., Suzuki-Kamata, K., Matsuno, T., Ichihara, H., Seama, H., Kiyosugi, K., Nakaoka, R., Nakahigashi, K., Takizawa, H., Hayashi, K., Chiba, T., Shimizu, S., Sano, M., Iwamaru, H., Morozumi, H., Sugioka, H., and Yamamoto, Y., 2018. Giant rhyolite lava dome formation after 7.3 ka supereruption at Kikai caldera, SW Japan. *Scientific Report*, DOI:10.1038/s41598-018-21066-w.

- Ui, T., 1973. Koya pyroclastic flow – a discovery of unusually widespread and thin pyroclastic deposits. *Bulletin of the Volcanology Society of Japan* 18, 153-168.
- Vacquier, V., 1985. The measurement of thermal conductivity of solids with a transient linear heat source on the plane surface of a poorly conducting body. *Earth and Planetary Science Letters*, 74, 275-279.
- Von Herzen, R. and Maxwell, A. E, 1959. The measurement of thermal conductivity of deep-sea sediments by a needle-probe method. *Journal of Geophysical Research*, 64, 1557-1563